

Hard-sphere interactions in velocity jump models

Benjamin Franz,^{1,*} Jake Taylor-King,¹ Christian Yates,² and Radek Erban^{1,†}

¹*Mathematical Institute, University of Oxford, Radcliffe Observatory Quarter,
Woodstock Road, Oxford OX2 6GG, United Kingdom*

²*Department of Mathematical Sciences, University of Bath,
Claverton Down, Bath BA2 7AY, United Kingdom*

(Dated: June 10, 2016)

Group-level behaviour of particles undergoing a velocity jump process with hard-sphere interactions is investigated. We derive N -particle transport equations that include the possibility of collisions between particles and apply different approximation techniques to get expressions for the dependence of the collective diffusion coefficient on the number of particles and their diameter. The derived approximations are compared with numerical results obtained from individual-based simulations. The theoretical results compare well with Monte Carlo simulations providing the excluded volume fraction is small.

I. INTRODUCTION

We study the effect of hard-sphere collisions on the behaviour of groups of particles moving according to a velocity jump process, meaning that particles follow a given velocity and switch to a different velocity at randomly distributed times [1]. Velocity jump processes are often used to model movement of biological individuals, including the bacterium *E. coli* [2] and reef fish larvae [3]. Additionally, these random walks can be applied to target-finding problems in swarm robotics studies [4].

If collisions between particles are neglected, then the velocity jump process can be described using the transport equation [1]

$$\frac{\partial q}{\partial t} + \mathbf{v} \cdot \nabla_{\mathbf{x}} q = -\lambda q + \lambda \int_V T(\mathbf{v}, \mathbf{u}) q(t, \mathbf{x}, \mathbf{u}) d\mathbf{u}, \quad (1)$$

where $q(t, \mathbf{x}, \mathbf{v})$ represents the concentration of particles that are located at position $\mathbf{x} \in \mathbb{R}^d$ and moving with velocity $\mathbf{v} \in \mathbb{R}^d$, $d = 2, 3$, at time $t > 0$, and $\lambda > 0$ is the turning frequency. The turning kernel $T(\mathbf{v}, \mathbf{u})$ in (1) gives the probability density of turning from velocity \mathbf{u} to velocity \mathbf{v} , given that a reorientation occurs [1]. The probability distribution specifying the time between turning events is exponential with mean λ^{-1} (for non-exponentially distributed reorientation events, see [5, 6]). The main aim of this paper is to incorporate hard-sphere particle interactions into the velocity jump equation (1).

In the physical literature the effect of interactions on diffusion processes has been studied for a long time [7]. Ohtsuki and Okano [8] consider the difference between collective and individual diffusivity and show that both behave differently under the influence of interactions. In particular they show that interactions lead to enhanced collective diffusion, but reduced individual diffusion. Bruna and Chapman [9] derive similar results using the technique of matched asymptotic expansions for

particles in non-confined spaces. Their results are further extended for multiple species [10] and for particles in confined spaces [11]. Recently the effect of crowded environments on diffusivity has been studied using individual-based particle simulations [12] and comparing those to experimental results [13]. The effect of macromolecular (intracellular) crowding on reaction rates has also been studied in the biological literature [14–16]. Comparisons between experimental and model results have been used by Hall and Minton [17] to derive rate laws. This effect can have a significant influence on the accuracy of *in vivo* experiments [18], as those often cannot fully represent crowding effects present in physiological media [19].

The kinetic behaviour of ideal gases can also be interpreted as a velocity jump process with collisions, albeit here the frequency of self turning (i.e. turning given by rate λ in equation (1)) vanishes [20]. In these gases, interactions occur in the form of fully elastic collisions, i.e. momentum is conserved during a collision. In this paper, we are, however, interested in systems where all particles always move with the speed $s \in \mathbb{R}^+$. Therefore we consider the so-called reflective (speed-preserving) collisions [4]. In this type of interaction particles get directly reflected off each other with the individual speed of each particle being conserved. Whilst this type of collisions does not appear in kinetic theory, it can still be applied to a number of biologically relevant systems. In [21], the formation of fish swarms is studied and reflective collisions play an important part in this model. Reflective collisions are also easy to implement in swarm robotics applications [4].

The two types of collisions are illustrated in Figure 1. In both cases, a particle at position \mathbf{x} and with velocity \mathbf{v} collides with a second particle at $\mathbf{x} + \varepsilon \mathbf{n}$ that has velocity \mathbf{u} , where $\mathbf{n} \in \mathbb{S}^{d-1}$ is a unit vector. Here, ε describes the (identical) diameter of each of the particles. We denote the velocities after the collision took place by \mathbf{v}' and \mathbf{u}' respectively. For the reflective (speed-preserving) collisions, we assume that

$$\mathbf{v}' = \mathbf{v} - 2(\mathbf{v} \cdot \mathbf{n}) \mathbf{n}, \quad \mathbf{u}' = \mathbf{u} - 2(\mathbf{u} \cdot \mathbf{n}) \mathbf{n}. \quad (2)$$

* bfranz@google.com

† erban@maths.ox.ac.uk

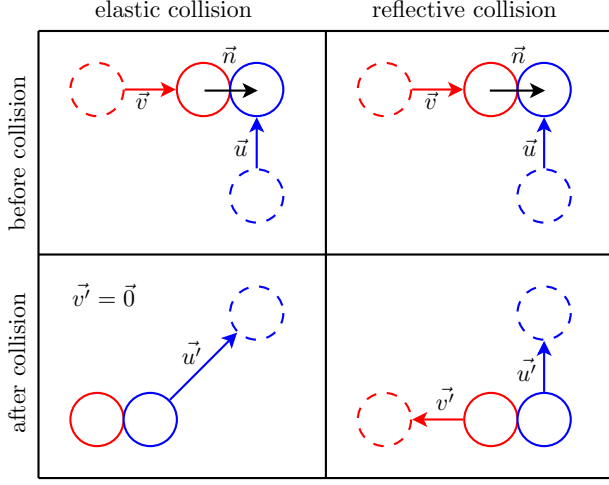


FIG. 1. Comparison between elastic collision (3) (left panels) and reflective collision (2) (right panels). The velocities of the two particles before the collision are denoted as \mathbf{v}, \mathbf{u} , the velocities after the collision as \mathbf{v}', \mathbf{u}' and the normal of the collision surface as \mathbf{n} . The solid lines indicate the positions of the two particles at collision time, whilst the dashed lines show their positions before or after the collisions.

In the case of fully elastic collisions, the new velocities take the form

$$\mathbf{v}' = \mathbf{v} - ((\mathbf{v} - \mathbf{u}) \cdot \mathbf{n}) \mathbf{n}, \quad \mathbf{u}' = \mathbf{u} + ((\mathbf{v} - \mathbf{u}) \cdot \mathbf{n}) \mathbf{n}. \quad (3)$$

The main differences between these two types of collisions are that reflective collisions preserve speed, i.e. individuals travel at the same speed before and after the collision, whilst speeds typically change during fully elastic collisions; on the other hand, fully elastic collisions preserve total momentum in the system, whilst this is not the case for reflective collisions.

The remainder of the paper is organised as follows: In Section II we derive a transport equation for the system of interacting particles based on the BBGKY hierarchy [22, 23]. In Sections III and IV we then derive two approximative transport equations which generalize equation (1). In each case, we also present equations for effective diffusion constants. These approximations are then compared with the results obtained using individual-based simulations in Section V.

II. THE BBGKY HIERARCHY

In this section we derive transport equations for the N -particle system and later for the special case of a two-

particle system. These equations can be interpreted as the first equation of the BBGKY hierarchy [22, 23], a hierarchical system of transport equations that models the general kinetics of gases and liquids. Let us assume that we have a system of N identical particles with diameter ε situated inside the domain $\Omega \subset \mathbb{R}^d$, $d = 2, 3$. Each particle $i = 1, \dots, N$ is described by its position $\mathbf{x}_i \in \Omega$ and its velocity $\mathbf{v}_i \in V \subset \mathbb{R}^d$, where

$$V = \{\mathbf{v} \in \mathbb{R}^d \mid \|\mathbf{v}\| = s\} \quad (4)$$

is the *velocity space* and $s > 0$ is the constant speed of particles. The N particles undergo a velocity jump process with turning frequency $\lambda \in \mathbb{R}^+$ and turning kernel $T(\mathbf{v}, \mathbf{u})$. We define the N -particle group state vectors by

$$\vec{\mathbf{x}} = (\mathbf{x}_1, \dots, \mathbf{x}_N), \quad \text{and} \quad \vec{\mathbf{v}} = (\mathbf{v}_1, \dots, \mathbf{v}_N).$$

Then we can write an N -particle transport equation for the group density function $Q(t, \vec{\mathbf{x}}, \vec{\mathbf{v}})$ as follows

$$\begin{aligned} & \left(\frac{\partial}{\partial t} + \sum_{i=1}^N \mathbf{v}_i \cdot \nabla_{\mathbf{x}_i} + \lambda N \right) Q(t, \vec{\mathbf{x}}, \vec{\mathbf{v}}) \\ &= \lambda \sum_{i=1}^N \int_V T(\mathbf{v}_i, \mathbf{v}_*) \\ & \quad \times Q\left(t, \vec{\mathbf{x}}, \mathbf{v}_1, \dots, \mathbf{v}_{i-1}, \mathbf{v}_*, \mathbf{v}_{i+1}, \dots, \mathbf{v}_N\right) d\mathbf{v}_*. \end{aligned} \quad (5)$$

This transport equation is valid in the region $\vec{\mathbf{x}} \in \Omega_\varepsilon^N$ defined by

$$\Omega_\varepsilon^N = \{(\mathbf{x}_1, \dots, \mathbf{x}_N) \in \Omega^N : \|\mathbf{x}_i - \mathbf{x}_j\| \geq \varepsilon, \forall i \neq j\}.$$

Collisions between two particles happen with a probability $\mathcal{O}(c)$, whilst collisions between three or more particles occur with probability $\mathcal{O}(c^2)$, where $c \sim N\varepsilon^d$ represents the total volume of the particles. Assuming that this volume is small compared to the size of the domain Ω , two-particle collisions represent the leading order behaviour and interactions between more than two particles can be neglected. We will therefore concentrate on the two-particle case of (5) that takes the form [34]:

$$\underbrace{\frac{\partial Q}{\partial t}}_{(i)} + \underbrace{\mathbf{v} \cdot \nabla_{\mathbf{x}} Q}_{(ii)} + \underbrace{\mathbf{u} \cdot \nabla_{\mathbf{y}} Q}_{(iii)} = \underbrace{-2\lambda Q}_{(iv)} + \underbrace{\lambda \int_V T(\mathbf{v}, \mathbf{v}_*) Q(t, \mathbf{x}, \mathbf{y}, \mathbf{v}_*, \mathbf{u}) d\mathbf{v}_*}_{(v)} + \underbrace{\lambda \int_V T(\mathbf{u}, \mathbf{u}_*) Q(t, \mathbf{x}, \mathbf{y}, \mathbf{v}, \mathbf{u}_*) d\mathbf{u}_*}_{(vi)}. \quad (6)$$

The two-particle density function is subject to the reflective external boundary conditions

$$\begin{aligned} Q(t, \mathbf{x}, \mathbf{y}, \mathbf{v}, \mathbf{u}) &= Q(t, \mathbf{x}, \mathbf{y}, \hat{\mathbf{v}}, \mathbf{u}), & \mathbf{x} \in \partial\Omega, \\ Q(t, \mathbf{x}, \mathbf{y}, \mathbf{v}, \mathbf{u}) &= Q(t, \mathbf{x}, \mathbf{y}, \mathbf{v}, \hat{\mathbf{u}}), & \mathbf{y} \in \partial\Omega, \end{aligned} \quad (7)$$

where $\hat{\mathbf{v}}$ and $\hat{\mathbf{u}}$ are the reflected velocities for wall collisions given by

$$\hat{\mathbf{v}} = \mathbf{v} - 2(\mathbf{v} \cdot \mathbf{n})\mathbf{n},$$

where \mathbf{n} is the outwards-pointing normal vector at position $\mathbf{x} \in \partial\Omega$. Additionally, we impose the collision condition for all $\mathbf{x}, \mathbf{y} \in \Omega$ with $\|\mathbf{x} - \mathbf{y}\| = \varepsilon$

$$Q(t, \mathbf{x}, \mathbf{y}, \mathbf{v}, \mathbf{u}) = Q(t, \mathbf{x}, \mathbf{y}, \mathbf{v}', \mathbf{u}'), \quad (8)$$

where the velocities after collision \mathbf{v}', \mathbf{u}' are defined in (2). In order to derive a one-particle transport equation similar to the classical velocity jump equation in (1), we integrate over the coordinates of the second particle. In particular, we integrate with respect to $\mathbf{u} \in V$ and $\mathbf{y} \in \Omega_2$ given by

$$\Omega_2 \equiv \Omega_2(\mathbf{x}) = \{\mathbf{y} \in \Omega : \|\mathbf{x} - \mathbf{y}\| \geq \varepsilon\}.$$

We then define the one-particle density as follows

$$q(t, \mathbf{x}, \mathbf{v}) = \int_{\Omega_2} \int_V Q(t, \mathbf{x}, \mathbf{y}, \mathbf{v}, \mathbf{u}) \, d\mathbf{u} \, d\mathbf{y}.$$

Integrating each component (i)–(vi) in (6) individually, we can derive the one-particle transport equation.

(i): Since the domain, Ω_2 , and the velocity space, V , do not depend explicitly on time, we can bring the time derivative outside the integral to obtain

$$\int_{\Omega_2} \int_V \frac{\partial Q}{\partial t} \, d\mathbf{u} \, d\mathbf{y} = \frac{\partial q}{\partial t}.$$

(ii): We use Reynolds' transport theorem in space to obtain

$$\begin{aligned} & \int_{\Omega_2(\mathbf{x})} \int_V \mathbf{v} \cdot \nabla_{\mathbf{x}} Q \, d\mathbf{u} \, d\mathbf{y} \\ &= \mathbf{v} \cdot \nabla_{\mathbf{x}} q - \int_{\partial B_\varepsilon(\mathbf{x})} \int_V (\mathbf{v} \cdot \mathbf{n}) Q(t, \mathbf{x}, \mathbf{y}, \mathbf{v}, \mathbf{u}) \, d\mathbf{u} \, d\mathbf{y}, \end{aligned}$$

where $B_\varepsilon(\mathbf{x})$ denotes the ball around \mathbf{x} with radius ε and \mathbf{n} is the outwards pointing normal vector. Note that in this case outwards is taken with respect to Ω_2 , hence \mathbf{n} in fact points into the ball $B_\varepsilon(\mathbf{x})$, i.e. it can be written as

$$\mathbf{n} = \frac{\mathbf{x} - \mathbf{y}}{\|\mathbf{x} - \mathbf{y}\|}. \quad (9)$$

(iii): Using the divergence theorem, we obtain

$$\begin{aligned} & \int_{\Omega_2} \int_V \mathbf{u} \cdot \nabla_{\mathbf{y}} Q(t, \mathbf{x}, \mathbf{y}, \mathbf{v}, \mathbf{u}) \, d\mathbf{u} \, d\mathbf{y} \\ &= \int_{\partial\Omega \cup \partial B_\varepsilon(\mathbf{x})} \int_V (\mathbf{u} \cdot \mathbf{n}) Q(t, \mathbf{x}, \mathbf{y}, \mathbf{v}, \mathbf{u}) \, d\mathbf{u} \, d\mathbf{y}, \end{aligned}$$

where \mathbf{n} is again the outwards pointing normal vector with respect to Ω_2 which on the boundary segment $\partial B_\varepsilon(\mathbf{x})$ is given by (9). Using the boundary conditions along the wall $\partial\Omega$ given in (7) we can show that

$$\int_{\partial\Omega} \int_V (\mathbf{u} \cdot \mathbf{n}) Q(t, \mathbf{x}, \mathbf{y}, \mathbf{v}, \mathbf{u}) \, d\mathbf{u} \, d\mathbf{y} = 0.$$

(iv): One can simply integrate to obtain

$$-2\lambda \int_{\Omega_2} \int_V Q(t, \mathbf{x}, \mathbf{y}, \mathbf{v}, \mathbf{u}) \, d\mathbf{u} \, d\mathbf{y} = -2\lambda q(t, \mathbf{x}, \mathbf{v}).$$

(v): Switching the order of integration, we obtain

$$\begin{aligned} & \int_{\Omega_2} \int_V \lambda \int_V T(\mathbf{v}, \mathbf{v}_*) Q(t, \mathbf{x}, \mathbf{y}, \mathbf{v}_*, \mathbf{u}) \, d\mathbf{v}_* \, d\mathbf{u} \, d\mathbf{y} \\ &= \lambda \int_V T(\mathbf{v}, \mathbf{v}_*) q(t, \mathbf{x}, \mathbf{v}_*) \, d\mathbf{v}_*. \end{aligned}$$

(vi): We can again switch the order of integration and use $\int_V T(\mathbf{v}, \mathbf{u}) \, d\mathbf{v} = 1$:

$$\begin{aligned} & \int_{\Omega_2} \int_V \lambda \int_V T(\mathbf{u}, \mathbf{u}_*) Q(t, \mathbf{x}, \mathbf{y}, \mathbf{v}, \mathbf{u}_*) \, d\mathbf{u}_* \, d\mathbf{u} \, d\mathbf{y} \\ &= \lambda \int_{\Omega_2} \int_V \int_V T(\mathbf{u}, \mathbf{u}_*) \, d\mathbf{u} \, Q(t, \mathbf{x}, \mathbf{y}, \mathbf{v}, \mathbf{u}_*) \, d\mathbf{u}_* \, d\mathbf{y} \\ &= \lambda \int_{\Omega_2} \int_V Q(t, \mathbf{x}, \mathbf{y}, \mathbf{v}, \mathbf{u}_*) \, d\mathbf{u}_* \, d\mathbf{y} = \lambda q(t, \mathbf{x}, \mathbf{v}). \end{aligned}$$

Summing the results in (i)–(vi), the one-particle transport equation takes the form

$$\begin{aligned} \frac{\partial q}{\partial t} + \mathbf{v} \cdot \nabla_{\mathbf{x}} q &= -\lambda q + \lambda \int_V T(\mathbf{v}, \mathbf{v}_*) q(t, \mathbf{x}, \mathbf{v}_*) \, d\mathbf{v}_* \\ &+ \int_{\partial B_\varepsilon(\mathbf{x})} \int_V Q(t, \mathbf{x}, \mathbf{y}, \mathbf{v}, \mathbf{u}) [\mathbf{n} \cdot (\mathbf{v} - \mathbf{u})] \, d\mathbf{u} \, d\mathbf{y}, \end{aligned}$$

where $\mathbf{n} = (\mathbf{x} - \mathbf{y})/\varepsilon$ is a normal vector. Inverting from \mathbf{n} to $-\mathbf{n}$ in the last term, \mathbf{y} can be written as $\mathbf{y} = \mathbf{x} + \varepsilon\mathbf{n}$ and we can transform the integral over the surface of the ball $B_\varepsilon(\mathbf{x})$ into an integral over the surface of unit sphere \mathbb{S}^{d-1} in d dimensions

$$\begin{aligned} \frac{\partial q}{\partial t} + \mathbf{v} \cdot \nabla_{\mathbf{x}} q &= -\lambda q + \lambda \int_V T(\mathbf{v}, \mathbf{v}_*) q(t, \mathbf{x}, \mathbf{v}_*) \, d\mathbf{v}_* \\ &- \varepsilon^{d-1} \int_{\mathbb{S}^{d-1}} \int_V Q(t, \mathbf{x}, \mathbf{x} + \varepsilon\mathbf{n}, \mathbf{v}, \mathbf{u}) [\mathbf{n} \cdot (\mathbf{v} - \mathbf{u})] \, d\mathbf{u} \, d\mathbf{n}, \end{aligned}$$

where the sign the collision term changes because of the flip from \mathbf{n} to $-\mathbf{n}$. Because the influence of collisions of more than two particles is negligible, as discussed, we can generalise this equation for N particles by simply adding up the influences of each of the other $(N - 1)$ particles and we obtain

$$\begin{aligned} \frac{\partial q}{\partial t} + \mathbf{v} \cdot \nabla_{\mathbf{x}} q &= -\lambda q + \lambda \int_V T(\mathbf{v}, \mathbf{v}_*) q(t, \mathbf{x}, \mathbf{v}_*) \, d\mathbf{v}_* \\ &- \kappa \int_{\mathbb{S}^{d-1}} \int_V Q(t, \mathbf{x}, \mathbf{x} + \varepsilon\mathbf{n}, \mathbf{v}, \mathbf{u}) [\mathbf{n} \cdot (\mathbf{v} - \mathbf{u})] \, d\mathbf{u} \, d\mathbf{n}, \end{aligned} \quad (10)$$

where we define $\kappa = \varepsilon^{d-1}(N-1)$. In order to analyse this equation further, we define the subsets of \mathbb{S}^{d-1}

$$\mathbb{S}_+^{d-1} \equiv \mathbb{S}_+^{d-1}(\mathbf{v} - \mathbf{u}) = \{\mathbf{n} \in \mathbb{S}^{d-1} : \mathbf{n} \cdot (\mathbf{v} - \mathbf{u}) > 0\}.$$

We can now split the collision integral in the transport equation (10) into integral over \mathbb{S}_+^{d-1} and $\mathbb{S}^{d-1} \setminus \mathbb{S}_+^{d-1}$ and apply the boundary conditions given in (8). We obtain

$$\begin{aligned} & -\kappa \int_{\mathbb{S}^{d-1}} \int_V Q(t, \mathbf{x}, \mathbf{x} + \varepsilon \mathbf{n}, \mathbf{v}, \mathbf{u}) [\mathbf{n} \cdot (\mathbf{v} - \mathbf{u})] \, d\mathbf{u} \, d\mathbf{n} \\ & = -\kappa \int_{\mathbb{S}_+^{d-1}} \int_V Q(t, \mathbf{x}, \mathbf{x} + \varepsilon \mathbf{n}, \mathbf{v}, \mathbf{u}) [\mathbf{n} \cdot (\mathbf{v} - \mathbf{u})] \, d\mathbf{u} \, d\mathbf{n} \\ & \quad \kappa \int_{\mathbb{S}_+^{d-1}} \int_V Q(t, \mathbf{x}, \mathbf{x} - \varepsilon \mathbf{n}, \mathbf{v}', \mathbf{u}') [\mathbf{n} \cdot (\mathbf{v} - \mathbf{u})] \, d\mathbf{u} \, d\mathbf{n}. \end{aligned}$$

Substituting this into (10), we obtain

$$\begin{aligned} \frac{\partial q}{\partial t} + \mathbf{x} \cdot \nabla_{\mathbf{x}} q &= -\lambda q + \lambda \int_V T(\mathbf{v}, \mathbf{u}) q(t, \mathbf{x}, \mathbf{u}) \, d\mathbf{u} \\ & + \kappa \int_{\mathbb{S}_+^{d-1}} \int_V \left[Q(t, \mathbf{x}, \mathbf{x} - \varepsilon \mathbf{n}, \mathbf{v}', \mathbf{u}') \right. \\ & \quad \left. - Q(t, \mathbf{x}, \mathbf{x} + \varepsilon \mathbf{n}, \mathbf{v}, \mathbf{u}) \right] [\mathbf{n} \cdot (\mathbf{v} - \mathbf{u})] \, d\mathbf{u} \, d\mathbf{n}. \end{aligned} \quad (11)$$

The problem we face now is that this equation still contains the two-particle density function Q , which is unknown. In the following two sections we will discuss how this issue can be resolved through approximation of the two-particle density. Note the small subtlety that one typically approximates the two-particle density *before* applying boundary conditions, thus one only needs the chosen approximation before collision events, and not after. We make the derivation in this order so one can place greater emphasis on the two-particle density approximation.

For the remainder of this paper we will concentrate on a two-dimensional environment, which helps evaluating many of the integrals that occur in the derivations. The general ideas could be applied for $d = 3$, but the evaluation of the integrals might prove significantly more difficult. Applications of the two-dimensional analysis include swarm robotics studies with differential wheeled robots [4].

III. BOLTZMANN COLLISION INTEGRAL

We consider a two-dimensional system (i.e. $d = 2$) in the dilute gas limit given by

$$N \rightarrow \infty, \quad \varepsilon \rightarrow 0, \quad (N-1)\varepsilon = \kappa. \quad (12)$$

Note that in this limit the system is dilute in the sense that the area fraction $c \sim N\varepsilon^2$ vanishes [24]. In this section we use the molecular chaos assumption which states that velocities are locally independent of each other, and we can write [20]

$$Q(t, \mathbf{x}, \mathbf{y}, \mathbf{v}, \mathbf{u}) = q(t, \mathbf{x}, \mathbf{v}) q(t, \mathbf{y}, \mathbf{u}), \quad (13)$$

for all $\mathbf{x}, \mathbf{y} \in \Omega$ and $\mathbf{v}, \mathbf{u} \in V$. Substituting this into (11) and using (12), we obtain an equation that contains the so-called *Boltzmann integral* as the last term [20]

$$\begin{aligned} \frac{\partial q}{\partial t} + \mathbf{v} \cdot \nabla_{\mathbf{x}} q &= -\lambda q + \lambda \int_V T(\mathbf{v}, \mathbf{u}) q(t, \mathbf{x}, \mathbf{u}) \, d\mathbf{u} \\ & + \kappa \int_{\mathbb{S}_+^1} \int_V \left[q(t, \mathbf{x}, \mathbf{v}') q(t, \mathbf{x}, \mathbf{u}') \right. \\ & \quad \left. - q(t, \mathbf{x}, \mathbf{v}) q(t, \mathbf{x}, \mathbf{u}) \right] [\mathbf{n} \cdot (\mathbf{v} - \mathbf{u})] \, d\mathbf{u} \, d\mathbf{n}. \end{aligned} \quad (14)$$

Next, we use the Cattaneo approximation [25] to derive the effective diffusion properties of the hard-sphere velocity jump process. This approximation is based on an L^2 moment-closure of a hierarchy of equations for the various velocity moments of the mesoscopic density $q(t, \mathbf{x}, \mathbf{v})$. The equation for the zeroth moment (particle density)

$$\varrho \equiv \varrho(t, \mathbf{x}) = \int_V q(t, \mathbf{x}, \mathbf{v}) \, d\mathbf{v}$$

is derived by integrating (14) with respect to $\mathbf{v} \in V$. Due to symmetry in \mathbf{u} and \mathbf{v} the Boltzmann collision term vanishes in this equation and we obtain the conservation of mass property

$$\frac{\partial \varrho}{\partial t} + \nabla_{\mathbf{x}} \cdot \mathbf{m}^{(1)} = 0 \quad (15)$$

where $\mathbf{m}^{(1)}$ is the first velocity moment

$$\mathbf{m}^{(1)} = \int_V \mathbf{v} q(t, \mathbf{x}, \mathbf{v}) \, d\mathbf{v}.$$

Whilst mass is conserved in the system, momentum is not due to the nature of the collisions and the randomly distributed self-turns. This can, for example, be seen easily in Figure 1. However, energy is conserved in the system, due to the conservation of mass combined with the fact that all particles conserve their speed $\|\mathbf{v}\| = s$ at all times. Multiplying (14) with \mathbf{v} and then integrating with respect to $\mathbf{v} \in V$ we obtain an equation for the first moment $\mathbf{m}^{(1)}$. This equation is identical to results seen in [25] for a non-interacting velocity jump processes, except for the influence of the Boltzmann collision term in (14). This difference is given by the integral

$$\begin{aligned} I &= \underbrace{\int_V \int_V \int_{\mathbb{S}_+^1} \mathbf{v} q(\mathbf{v}') q(\mathbf{u}') (\mathbf{v} - \mathbf{u}) \cdot \mathbf{n} \, d\mathbf{n} \, d\mathbf{u} \, d\mathbf{v}}_{I_1} \\ &\quad - \int_V \int_V \int_{\mathbb{S}_+^1} \mathbf{v} q(\mathbf{v}) q(\mathbf{u}) (\mathbf{v} - \mathbf{u}) \cdot \mathbf{n} \, d\mathbf{n} \, d\mathbf{u} \, d\mathbf{v}. \end{aligned} \quad (16)$$

In Appendix A we approximate this integral to (see (A3))

$$I \approx \frac{32s}{9\pi} \varrho \mathbf{m}^{(1)}.$$

Hence, the equation for the first velocity moment takes the approximate form

$$\frac{\partial \mathbf{m}^{(1)}}{\partial t} + \nabla_{\mathbf{x}} M^{(2)} = -\mathbf{m}^{(1)} \left(\lambda + s\kappa \frac{32}{9\pi} \varrho \right), \quad (17)$$

where the second velocity moment is defined by

$$M^{(2)} = \int_V \mathbf{v} \mathbf{v}^T q(t, \mathbf{x}, \mathbf{v}) d\mathbf{v}.$$

Following [25] we approximate $M^{(2)}$ by $s^2 \varrho \mathbb{I}/2$ where $\mathbb{I} \in \mathbb{R}^{2 \times 2}$ is the 2-dimensional identity matrix. Substituting this moment closure into (17), we obtain the second equation of the Cattaneo approximation in the form

$$\frac{\partial \mathbf{m}^{(1)}}{\partial t} + \frac{s^2}{2} \nabla_{\mathbf{x}} \varrho = -\mathbf{m}^{(1)} \left(\lambda + s\kappa \frac{32}{9\pi} \varrho \right). \quad (18)$$

Equations (15)–(18) form a closed system of three evolution equations for three unknowns (density ϱ and two components of $\mathbf{m}^{(1)}$). We can apply parabolic scaling limits as described in [26, 27] in order to obtain the effective density-dependent diffusivity of the system to be

$$D_{\text{eff},1}(\varrho) = \frac{s^2}{2(\lambda + s\kappa \frac{32}{9\pi} \varrho)}. \quad (19)$$

If we consider the original non-interacting unbiased velocity jump process (1), then the above analysis ($\kappa = 0$) leads to the effective diffusion constant $D_0 = s^2/2\lambda$. Using (19), we obtain $D_{\text{eff},1}(\varrho) \leq D_0$. This result will be further explored using numerical simulations in Section V. We formulate an alternative transport equation

as follows

$$\begin{aligned} \frac{\partial q}{\partial t} + \mathbf{v} \cdot \nabla_{\mathbf{x}} q &= -\lambda_1 q + \lambda_1 \int_V T(\mathbf{v}, \mathbf{u}) q(\mathbf{u}) d\mathbf{u}, \\ \text{where } \lambda_1 &= \lambda + s\kappa \frac{32}{9\pi} \int_V q(\mathbf{v}) d\mathbf{v}. \end{aligned} \quad (20)$$

This adjusted transport equation corresponds to the effective diffusivity (19) and is used to numerically compare approximation (19) with individual-based simulations in Section V.

IV. MATCHED ASYMPTOTIC EXPANSION

We have used (13) together with dropping $\mathcal{O}(\varepsilon)$ terms to derive (14) from equation (11). In this section we keep the terms of order ε using the following approximation

$$\begin{aligned} Q(t, \mathbf{x}, \mathbf{x} \pm \varepsilon \mathbf{n}, \mathbf{v}, \mathbf{u}) &\sim q(t, \mathbf{x}, \mathbf{v}) q(t, \mathbf{x}, \mathbf{u}) \\ &\pm q(t, \mathbf{x}, \mathbf{v}) \varepsilon \mathbf{n} \cdot \nabla_{\mathbf{x}} q(t, \mathbf{x}, \mathbf{u}). \end{aligned}$$

Substituting into (11), we obtain a Boltzmann equation that has an additional $\mathcal{O}(\varepsilon)$ correction term and which we analyse using the method of matched asymptotic expansions [9]. Again, multiplying by \mathbf{v} and integrating with respect to $\mathbf{v} \in V$, we can derive the influence of this correction term on the Cattaneo approximation:

$$J = -\kappa\varepsilon \int_V \int_V \int_{\mathbb{S}_+^1} \mathbf{v} [q(\mathbf{v}') (\mathbf{n} \cdot \nabla_{\mathbf{x}} q(\mathbf{u}')) + q(\mathbf{v}) (\mathbf{n} \cdot \nabla_{\mathbf{x}} q(\mathbf{u}))] (\mathbf{v} - \mathbf{u}) \cdot \mathbf{n} d\mathbf{n} d\mathbf{u} d\mathbf{v}. \quad (21)$$

Following the derivation in Appendix B, we obtain:

$$J \approx -\kappa\varepsilon \frac{\pi s^2}{2} \varrho \nabla_{\mathbf{x}} \varrho.$$

Plugging all the corrections into the second equation of the Cattaneo approximation, we arrive at

$$\frac{\partial \mathbf{m}^{(1)}}{\partial t} + \frac{s^2}{2} \nabla_{\mathbf{x}} \varrho (1 + \kappa\varepsilon\pi\varrho) = -\mathbf{m}^{(1)} \left(\lambda + s\kappa \frac{32}{9\pi} \varrho \right),$$

and therefore, using the parabolic scaling limit again [26, 27], we derive the effective diffusivity

$$D_{\text{eff},2}(\varrho) = \frac{s^2 (1 + \kappa\varepsilon\pi\varrho)}{2(\lambda + s\kappa \frac{32}{9\pi} \varrho)}. \quad (22)$$

We can see that, depending on the parameter regime, $D_{\text{eff},2}$ can be higher or lower than diffusivity of point particles given through $D_0 = s^2/2\lambda$. For low volume fractions, $\kappa\varepsilon$, we recover (19) and therefore a lower group diffusivity than point particles. As volume fraction increases though, the group diffusivity can actually be

larger than that of point particles. These effects will be discussed in more detail in Sections V and VI. Note also that this effective diffusivity is larger than the effective diffusivity obtained for the Boltzmann-like equation (14) for all values of $\varepsilon > 0$ and hence that the finite size of particles accelerates the diffusion process. We can again formulate an adjusted velocity jump process, as we did in equation (20), as

$$\begin{aligned} \frac{\partial q}{\partial t} + \mathbf{v} \cdot \nabla_{\mathbf{x}} q &= -\lambda_2 q + \lambda_2 \int_V T(\mathbf{v}, \mathbf{u}) q(\mathbf{u}) d\mathbf{u}, \\ \text{where } \lambda_2 &= \frac{\lambda + s\kappa \frac{32}{9\pi} \int_V q(\mathbf{v}) d\mathbf{v}}{1 + \kappa\varepsilon\pi \int_V q(\mathbf{v}) d\mathbf{v}}. \end{aligned} \quad (23)$$

To verify this adjusted equation, we will compare it numerically to individual-based simulations in Section V.

V. SIMULATION RESULTS

In Sections III and IV, we have presented a total of three different models that we want to compare to individual-

based simulations. The three models are given by (i) the Boltzmann-like equation (14), (ii) the first adjusted velocity jump model (20) that approximates the Boltzmann term, and (iii) the second adjusted velocity jump model (23) that was derived using the method of matched asymptotic expansions. All individual-based simulations are performed using an event-based kinetic Monte-Carlo (KMC) [28] simulation of the velocity jump processes. The main idea of this algorithm is that one can jump directly from one event to the other without missing events. Models (i) and (ii) are valid only in the dilute gas limit, i.e. we can only expect those to compare well to KMC simulations for very small values of the area fraction c . Model (iii) on the other hand should give good comparisons even for larger values of c .

We begin with investigating the collision frequency in Section V A. We compare the KMC results with the results predicted by the Boltzmann equation. Then we compare numerical solutions of all three models with KMC simulations in Sections V B and V C. They are solved using a first order explicit finite volume scheme in a unit square domain $\Omega = [-0.5, 0.5] \times [-0.5, 0.5]$. We discretise the velocity space into 40 velocity directions and use a grid size of $\Delta x = 0.005$ and a time step of $\Delta t = 10^{-4}$. The initial condition is given by

$$q(0, \mathbf{x}, \mathbf{v}) = \begin{cases} \frac{16}{\pi |V|} & \text{for } \|\mathbf{x}\| \leq \frac{1}{4}, \mathbf{v} \in V, \\ 0, & \text{otherwise.} \end{cases} \quad (24)$$

meaning that particles are uniformly distributed in the ball of radius $1/4$ around the origin with uniformly distributed velocities. For KMC simulations we apply a re-sampling procedure to ensure none-overlapping particles. In all simulations, we run the system until $t = 0.05$ and use the parameter values $\lambda = 200$ and $s = 20$.

A. Numerical study of collision frequency

In this first study, we perform numerical experiments that count the frequency of collisions from an individual perspective. We use a unit square with periodic boundary conditions in order to avoid boundary influences. In these experiments the number of direction changes due to collisions in the system is counted for a certain amount of time and then divided by the number of particles and by the run-time. The area fraction c and the collision parameter κ are given by

$$\kappa = (N - 1)\varepsilon, \quad \text{and} \quad c = \frac{1}{4}N\pi\varepsilon^2. \quad (25)$$

For a given pair (κ, c) , the nearest integer value N and an adequate value of ε is found and an experiment is performed. In Figure 2(a), we can see how the collision frequency λ_{coll} depends on the value of κ and is on a leading order scale independent of c . We have a linear

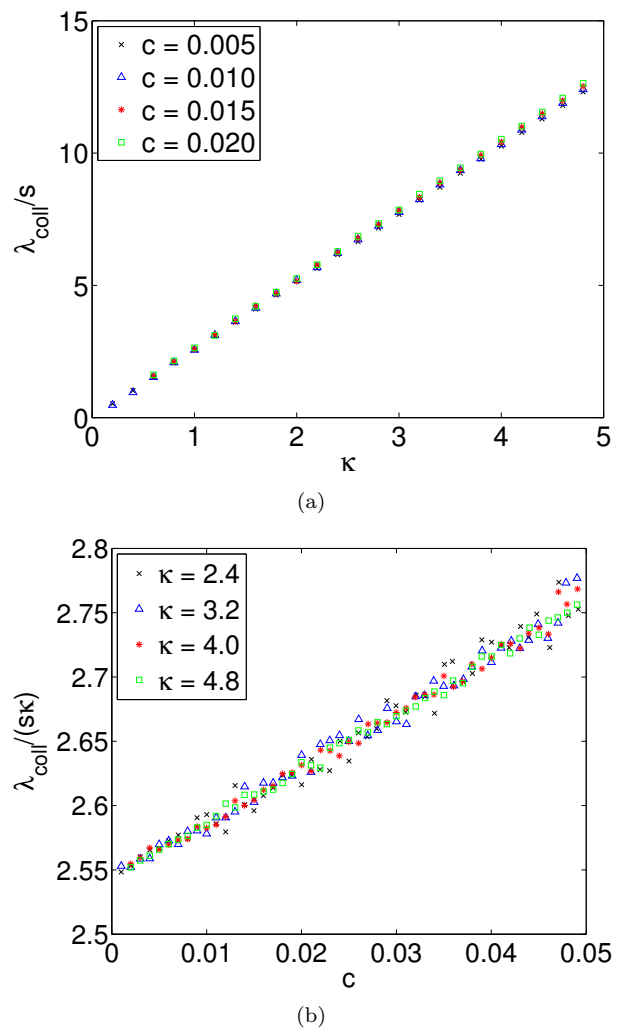


FIG. 2. (a) The dependence of collision frequency, λ , on κ for different values of c . (b) The dependence of collision frequency divided by κ (i.e. $\lambda_{\text{coll}}/s\kappa$) on c for different values of κ . For both plots parameters and numerical methods are given in the text.

relationship, which can be estimated as

$$\lambda_{\text{coll}} \approx 2.55 s \kappa.$$

The linear dependence on s is necessary, seeing that an increase in particle speed is equivalent to decreasing the run time of the system and vice-versa. Using results from the kinetic theory of gases [29], we can predict the frequency of collisions to be

$$\lambda_{\text{coll}} = 2 \varepsilon N \bar{v},$$

where \bar{v} is the mean relative velocity which can be computed by

$$\bar{v} = \frac{1}{|V|^2} \int_V \int_V \|\mathbf{v} - \mathbf{u}\| d\mathbf{v} d\mathbf{u} = \frac{4s}{\pi}.$$

#	N	ε	κ	c	Figure
(A)	1001	4×10^{-3}	4	1.26×10^{-2}	Figure 3
(B)	201	2×10^{-2}	4	6.31×10^{-2}	Figure 4

TABLE I. *Parameters for example simulations.*

Consequently, $\lambda_{\text{coll}} \approx 8 s \kappa / \pi \approx 2.55 s \kappa$, which provides an excellent match with the numerical results. We then use this information to get additional insight into the influence of the area fraction (concentration) c , by plotting the dependence of $\lambda_{\text{coll}}/s\kappa$ on c for different values of κ in Figure 2(b). Interestingly, for small concentrations ($c < 0.05$) this dependence does not change with κ and forms a monotonically increasing function, such that

$$\lambda_{\text{coll}} = \frac{8s}{\pi} \kappa f(c).$$

For the range of concentrations plotted in Figure 2(b), we can approximate $f(c)$ to be

$$f(c) \approx 1 + 1.73c.$$

This first numerical investigation demonstrates that at leading order the number of collisions depends linearly on κ , as predicted by the Boltzmann equation. Additionally, we show that a dependence on the area fraction is present. This dependence could be caused by grouping effects when more than two particles are close together and bump into each other repeatedly before they break up.

B. Distributions for two example simulations

In this section, we compare the three models with KMC simulations for the two test cases (A) and (B) as shown in Table I. Notably, in both of these test cases we have $\kappa = 4$. As Model (i) as given in (14) only depends on the value of κ and not otherwise on s or ε , this model will give the same result for both test cases (A) and (B) and we therefore only plot this result once. The same argument holds for Model (ii). The distributions can be seen in Figure 3 for problem (A) and Figure 4 for problem (B). In Figures 3(e) and 4(c), we show horizontal slices through the relevant distributions at $x_2 = 0.5$.

For case (A), we can see that all four plotted distributions look very similar and in particular all three Models (i)–(iii) seem to give a good approximation to the KMC results. One can attribute this similarity to the fact that example (A) contains a very small particle diameter ε and therefore a small volume fraction, i.e. it is close to the Boltzmann limit, where Models (i) and (ii) are accurate. However, when looking at the slice in Figure 3(e), we can already see that Model (iii) shown as the dash-dotted (green) line gives a much better approximation to the KMC simulations than the other two models. Additionally, we can see that the results of Models (i)

and (ii) match each other well, as expected. Diffusion in the KMC simulations seems to be enhanced compared to the Boltzmann limit, as predicted by (22).

For case (B), the results shown in Figure 4 indicate that the particles have spread considerably further than in case (A). As mentioned above, the corresponding simulations for Models (i) and (ii) were already shown in Panels (b) and (c) of Figure 3, respectively, and seem to differ greatly from the KMC results. This is confirmed in the slice plots in Figure 4(c), where neither Model (i) nor Model (ii) match well with the KMC results. The reason for this discrepancy is that the volume fraction in test problem (B) is not negligible and this system is therefore far from the dilute gas limit. Model (iii) shown as dash-dotted (green) line in Figure 4(c), on the other hand, shows a good match with the KMC simulations. This result confirms the validity of the adjusted system (23) as an approximation for particles undergoing a velocity jump process with reflective hard-sphere interactions in the considered parameter region.

C. Numerical comparison for changing parameter values

In order to further investigate the parameter regions in which each of the adjusted models gives a good match to the KMC simulations, we now perform a numerical investigation for varying parameter values. The condition that particles do not overlap during the initialisation process, presents a limit to the parameter regime we can investigate. The parameter values are shown in Table II.

In order to compare the distributions at the end of the simulation, we define the mean distance from the centre (MDC) for KMC simulations through

$$\langle \|\mathbf{x}_i - (0, 0)\| \rangle = \frac{1}{N} \sum_{i=1}^N \|\mathbf{x}_i\|.$$

During the simulations, we choose a number of runs such that N multiplied by the number of runs is at least 10^6 and take the average MDC over all those runs. The MDC for the PDE description takes the form

$$\frac{\int_{\Omega} \|\mathbf{x}\| \int_V q(t, \mathbf{x}, \mathbf{v}) d\mathbf{v} d\mathbf{x}}{\int_{\Omega} \int_V q(t, \mathbf{x}, \mathbf{v}) d\mathbf{v} d\mathbf{x}}.$$

Note that we explicitly only use this measure to compare the various distributions. We do not use this measure to derive diffusion constants and this measure does not correspond to the mean square displacement of particles during the simulation. This is important to note, because Bruna and Chapman [10] show that the mean square displacement is not an adequate measure for the collective diffusion constant, but for the self diffusion constant. However, because we are only using the MDC as a measure of the width of the distributions at the end of the simulations, it is a valid measure for the comparison between PDE Models (i)–(iii) and KMC simulations.

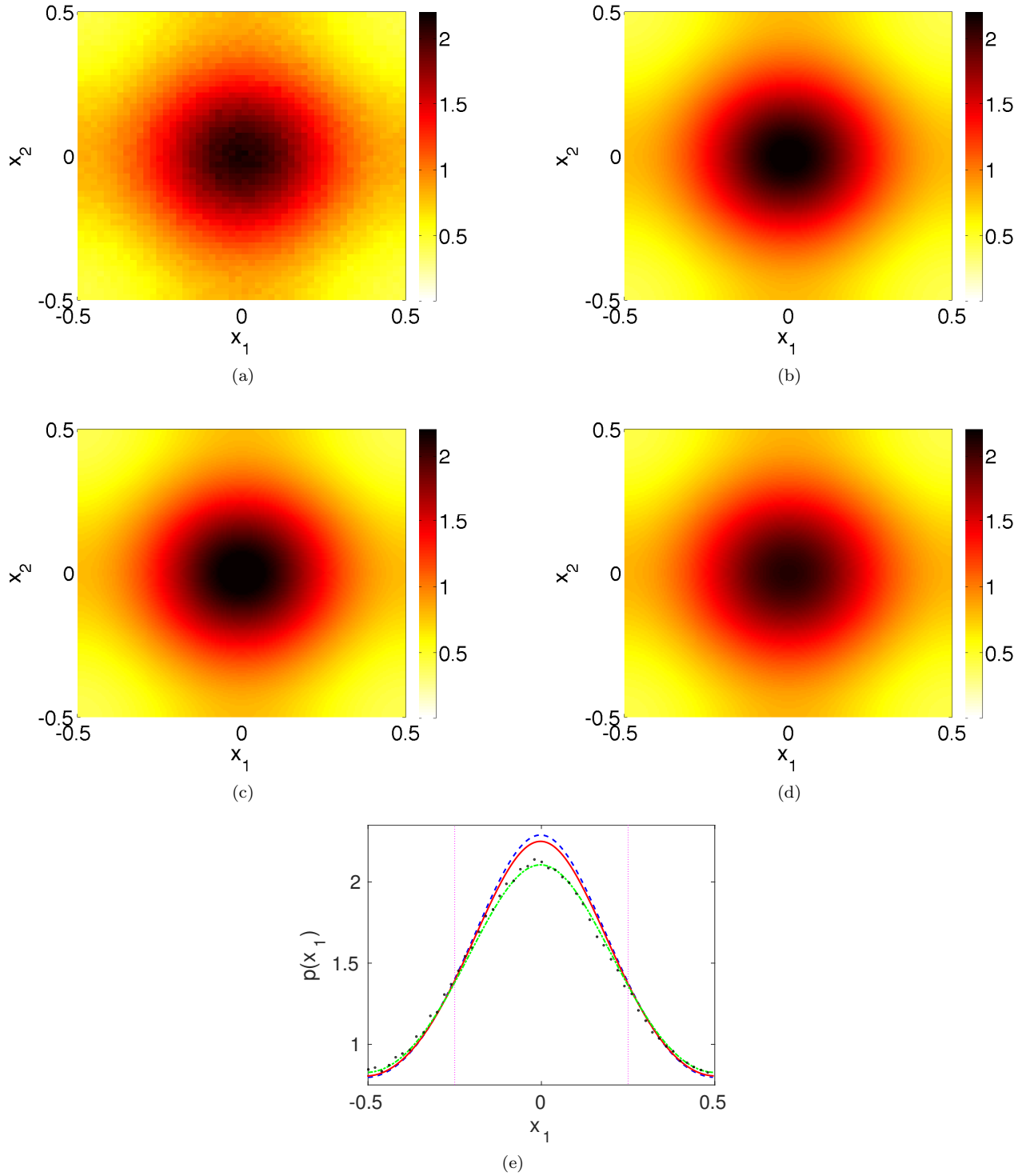


FIG. 3. Comparison between KMC simulation and numerical solutions of continuum approximations for the parameters $N = 1001$, $\varepsilon = 0.004$ and consequently $\kappa = 4$. We use the initial condition given in (24), zero-flux boundary conditions and plot distributions at time $t = 0.05$.

- (a) KMC simulation for 1001 particles of diameter $\varepsilon = 0.004$.
- (b) Numerical solution of Model (i) given by (14).
- (c) Numerical solution of Model (ii) given by (20).
- (d) Numerical solution of Model (iii) given by (23).
- (e) Slice through the distributions at $x_2 = 0$. Dashed (blue) line: Model (i); solid (red) line: Model (ii); dash-dotted (green) line: Model (iii); black circles: KMC simulation. Vertical dotted (purple) line indicates the initial condition.

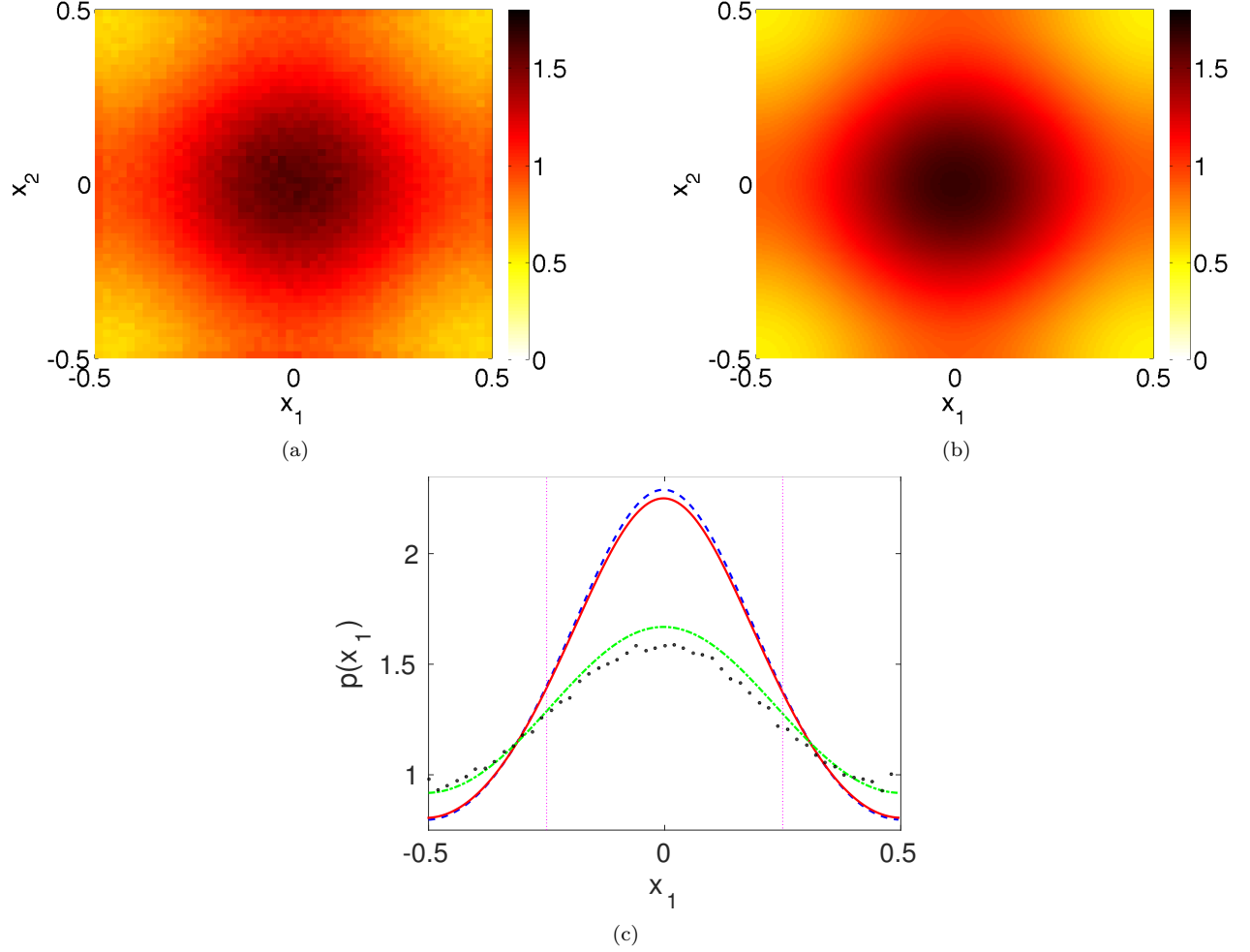


FIG. 4. Comparison between KMC simulation and numerical solutions of continuum approximations for the parameters $N = 201$, $\varepsilon = 0.02$ and consequently $\kappa = 4$. We use the initial condition given in (24), zero-flux boundary conditions and plot distributions at time $t = 0.05$.

- (a) KMC simulation for 201 particles of diameter $\varepsilon = 0.02$.
- (b) Numerical solution of Model (iii) given by (23).
- (c) Slice through the distributions at $x_2 = 0.5$. Dashed (blue) line: Model (i) (distribution given in Figure 3(b)); solid (red) line: Model (ii) (distribution given in Figure 3(c)); dash-dotted (green) line: Model (iii); black circles: KMC simulation. Vertical dotted (purple) line indicates the initial condition.

	N	ε	κ	c
Figure 5(a)	50	$0, \dots, 4 \times 10^{-2}$	$0, \dots, 1.96$	$0, \dots, 6.28 \times 10^{-2}$
Figure 5(b)	$1, \dots, 250$	2×10^{-2}	$0, \dots, 4.98$	$3.14 \times 10^{-4}, \dots, 7.82 \times 10^{-2}$
Figure 5(c)	$100, \dots, 2000$	$3 \times 10^{-2}, \dots, 1.5 \times 10^{-3}$	3	$7.21 \times 10^{-2}, \dots, 3.5 \times 10^{-3}$
Figure 5(d)	$6, \dots, 400$	$0.11, \dots, 1.26 \times 10^{-2}$	$0.55, \dots, 5.03$	5×10^{-2}

TABLE II. Parameter ranges for simulations in Figure 5.

The results of this comparison can be seen in Figure 5. In all four plots, the dotted (red) line indicates the uncorrected velocity jump equation (1) that does not consider collisions at all. The dashed (blue) line indicates the first correction given in (20) (Model (ii)) and the dash-dotted (green) line shows the second correction given in (23)

(Model (iii)). The (black) solid line shows the results obtained from KMC simulations. Note that we do not include Model (i) in this consideration, because the results are expected to be very similar to those of Model (ii).

In Figure 5(a) we plot the results for simulation runs with $N = 50$ and varying $\varepsilon \in [0, 0.04]$. We can see that

the MDC in KMC simulations, as well as in Model (iii), undergoes a non-monotonic behaviour with a minimum close to $\varepsilon = 0.02$. Model (ii) does not show such a behaviour, as κ is monotonically increasing with ε and diffusion is therefore increasingly slowed down. This model matches the KMC results well for very small values of ε , whilst Model (iii) provides a good match for values up to $\varepsilon \sim 0.02$. Above this value the KMC simulations and the second correction (23) start to diverge and one would need to consider further correction terms to achieve an accurate approximation in this regime. Interestingly for values of ε larger than about 0.034 the hard-sphere particles actually spread faster than point particles.

The second experiment shown in Figure 5(b) plots the dependence of MDC on N as we keep $\varepsilon = 0.02$ constant. We can see that the MDC decreases monotonically in the KMC simulations as well as in the PDE models. The first correction (20) does not provide a good match for N larger than about 5, whilst Model (iii) improves this match up to intermediate values of N . We see that for large values of $N > 100$ the KMC simulation spreads faster than both approximations, but slower than point particles.

Figure 5(c) presents the results for a constant value of κ . As is clear from the formulation of Model (ii) in (20), the first correction solely depends on κ and therefore provides a horizontal line in this case. The KMC simulations show higher values of MDC for lower values of N , i.e. in a regime far away from the Boltzmann limit. As we approach the Boltzmann limit when $N \rightarrow \infty$, the KMC simulations converge towards the value provided by Model (ii). As should be clear from the definition of Model (iii) in (23), the second approximation undergoes a similar behaviour and provides a very good match to the KMC simulations throughout.

In the last experiment we keep the area fraction of particles in the simulation constant, i.e. $c = \pi N \varepsilon^2 / 4 = 0.05$ and vary N and ε . The KMC simulations, as well as the PDE models, show monotonically decreasing values for the MDC throughout the considered parameter regime. Investigating the forms of the first and second corrections in (20) and (23) respectively, it becomes clear that the diffusion vanishes in the limit $N \rightarrow \infty$ when keeping the volume fraction constant. The reason for this is that κ goes to infinity in this limit. Therefore, we should expect the KMC results to converge towards the MDC of the initial condition for large values of N . In Figure 5(d), we can see that Model (ii) provides significantly different results to the KMC simulations in this regime that is far from the dilute gas limit. Model (iii) does not provide a perfect match to the simulation results either, but provides a significant improvement over Model (ii).

We conclude from this numerical study that the first approximation (Model (ii)) provides a good match to KMC simulations when a system close to the Boltzmann limit is considered. As one moves away from this limit and the area fraction becomes non-negligible, the second correction term (Model (iii)) provides an improved

match.

By far the largest and probably densest animal swarms are formed by desert locusts and contain around 50 million individuals per square kilometer [30]. Assuming a locust is an ellipse with major and minor axis of 7.5cm and 1cm, respectively, this results in a volume fraction of around 0.03, which according to the results in Figure 5 seems to be well within the range of volume fraction where (Model (iii)) provides accurate results, showing the potential biological relevance of this model.

VI. DISCUSSION

We have studied the effect of reflective collisions (2) on the diffusive behaviour of a group of particles that follow a velocity jump process. These reflective collisions differ from the fully elastic collisions (3) observed in gas molecules [29]. It is nevertheless interesting to study those reflective collisions, because they correspond more closely to behaviour seen in animal swarms [21, 31], where animals aim to avoid each other but evidently cannot transfer momentum. Reflective collisions conserve speed and can be used for modelling systems where all particles move with the same speed. We have studied such systems in this paper by assuming that the velocity space is given by (4). If we used elastic collisions (3), then some particles would have velocities $\mathbf{v}' \notin V$ after collisions. We would have to either adjust their speeds to s by modifying the running part of the velocity jump process, or remove these particles from the system. New particles with speed s would then have to be introduced to keep the number of particles N constant [32]. These technical issues have been avoided in this paper by using reflective collisions (2).

Starting from the BBGKY hierarchy [22, 23] we developed a number of PDE descriptions that we compared numerically to results obtained from individual-based KMC simulations. The first model we introduced stems from the Boltzmann equation [20] that is used in fluid flow simulations [33]. Using Cattaneo approximations [25] we then study the effect which the additional collision term has on the diffusive behaviour of the group of particles. We show that in the dilute gas limit collisions are always slowing down the collective diffusion. We then attempted to move away from the dilute gas limit and to introduce finite sized particles, using a matched asymptotic expansion approach adapted similar to that in [9]. Using the Cattaneo approximation again, we have derived equation (22) for the collective diffusion coefficient. This diffusion coefficient is larger than the one in the dilute gas limit. One can compare the results for velocity jump processes obtained in this work to the excluded volume methods in BD simulations [9] by considering the limit $s, \lambda \rightarrow \infty$, keeping $s^2/2\lambda = D_0$ constant. In this limit, the adjusted diffusion constant given by equation (22) takes the form $D_{\text{eff}}(\varrho) = D_0 (1 + \kappa \varepsilon \pi \varrho)$, which is indeed the form given by Bruna and Chapman

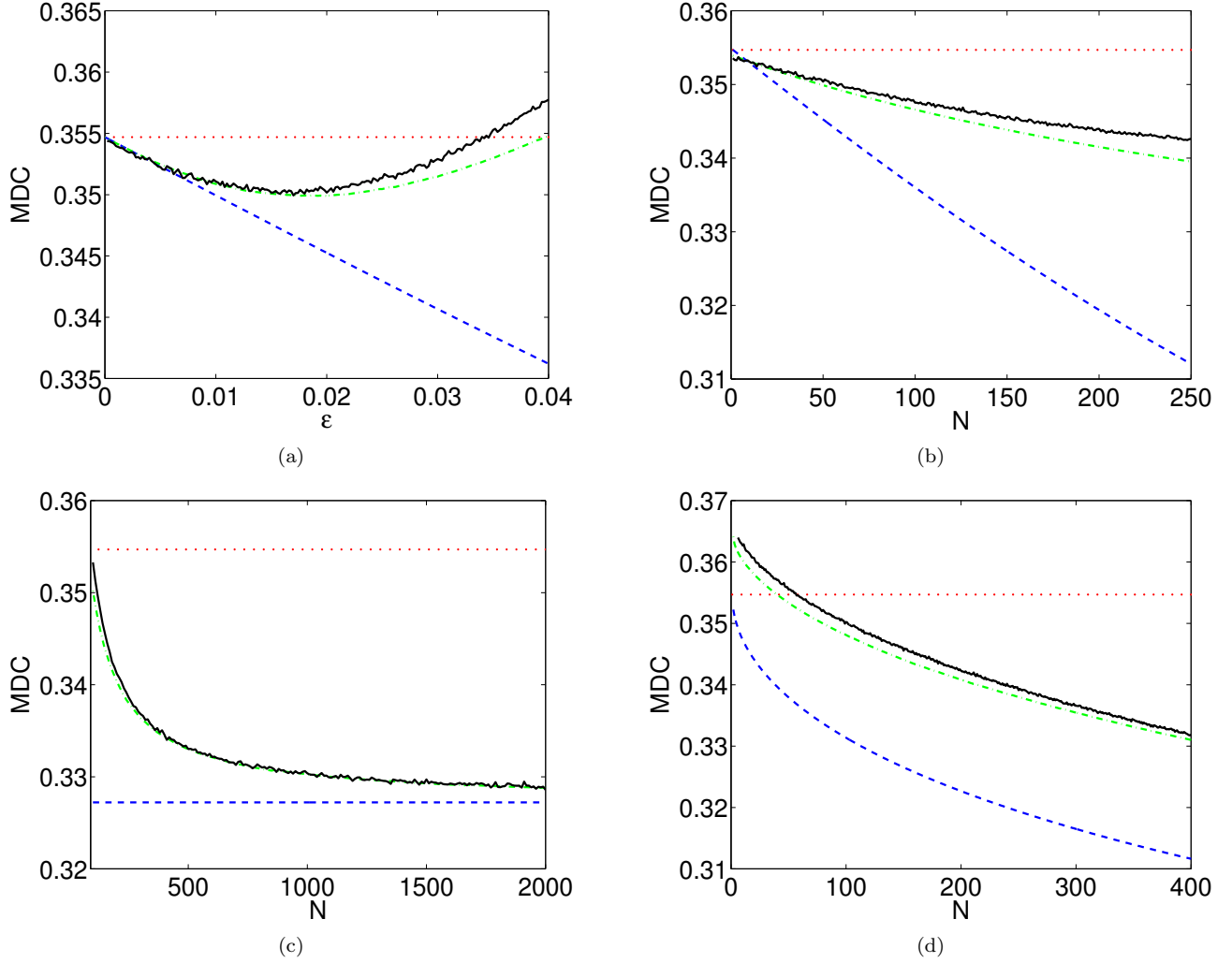


FIG. 5. Comparison between KMC simulation and numerical solutions of velocity jump processes with adjustments for collisions. Solid (black) line: KMC simulations; dotted (red) line: classical velocity jump equation (1); dashed (blue) line: Model (ii); dash-dotted (green) line: Model (iii). The simulation parameters are given in Table II.

[9, 10]. This indicates that the results shown in this paper are consistent with those for Brownian particles.

ACKNOWLEDGEMENTS

The research leading to these results has received funding from the European Research Council under the *European Community's* Seventh Framework Programme

(FP7/2007-2013) / ERC grant agreement No. 239870; and from the Royal Society through a Research Grant. Christian Yates would like to thank Christ Church, Oxford for support via a Junior Research Fellowship. Radek Erban would also like to thank the Royal Society for a University Research Fellowship; Brasenose College, University of Oxford, for a Nicholas Kurti Junior Fellowship; and the Leverhulme Trust for a Philip Leverhulme Prize.

-
- [1] H. Othmer, S. Dunbar, and W. Alt. Models of dispersal in biological systems. *Journal of Mathematical Biology*, 26:263–298, 1988.
- [2] H. Berg. *Random Walks in Biology*. Princeton University Press, 1983.

- [3] E. Codling, N. Hill, J. Pitchford, and S. Simpson. Random walk models for the movement and recruitment of reef fish larvae. *Marine Ecology Progress Series*, 279:215–224, 2004.
- [4] J. Taylor-King, B. Franz, C. Yates, and R. Erban. Mathematical modelling of turning delays in swarm robotics.

- IMA Journal of Applied Mathematics*, 80(5):1454–1474, 2015.
- [5] R. Friedrich, F. Janko, A. Baule and S. Eule. Exact solution of a generalized Kramer-Fokker-Planck equation retaining retardation effects. *Physical Review E*, 74:041103, 2006.
- [6] J. Taylor-King, E. van Loon, G. Rossner and S.J. Chapman. From birds to bacteria: generalised velocity jump processes with resting states. *Bulletin of Mathematical Biology*, 77(7):1213–1236, 2015.
- [7] B. Felderhof. Diffusion of interacting Brownian particles. *Journal of Physics A: Mathematical and General*, 11:929, 1978.
- [8] T. Ohtsuki and K. Okano. Diffusion coefficients of interacting Brownian particles. *The Journal of Chemical Physics*, 77(3):1443–1450, 1982.
- [9] M. Bruna and S. J. Chapman. Excluded-volume effects in the diffusion of hard spheres. *Physical Review E*, 85: 011103, 2012.
- [10] M. Bruna and S. J. Chapman. Diffusion of multiple species with excluded-volume effects. *The Journal of Chemical Physics*, 137:204116, 2012.
- [11] M. Bruna and S. J. Chapman. Diffusion of finite-size particles in confined geometries. *Bulletin of Mathematical Biology*, 76:947–982, 2014.
- [12] A. Ellery, M. Simpson, S. McCue, and R. Baker. Characterizing transport through a crowded environment with different obstacle sizes. *Journal of Chemical Physics*, 140: 054108, 2014.
- [13] E. Vilaseca, I. Pastor, S. Isvoran, A. Madurga, J.-Garces, and F. Mas. Diffusion in macromolecular crowded media: Monte Carlo simulation of obstructed diffusion vs. FRAP experiments. *Theoretical Chemistry Accounts*, 128:795–805, 2011.
- [14] R. Ellis. Macromolecular crowding: obvious but underappreciated. *Trends in Biochemical Sciences*, 26(10):597–604, 2001.
- [15] R. Grima and S. Schnell. A systematic investigation of the rate laws valid in intracellular environments. *Biophysical Chemistry*, 124:1–10, 2006.
- [16] M. Mourao, D. Kreitman, and S. Schnell. Unravelling the impact of obstacles in diffusion and kinetics of an enzyme catalysed reaction. *Physical Chemistry Chemical Physics*, 16:4492–4503, 2014.
- [17] D. Hall and A. Minton. Macromolecular crowding: qualitative and semiquantitative successes, quantitative challenges. *Biochimica et Biophysica Acta*, 1649:127–139, 2003.
- [18] S. Schnell and T. Turner. Reaction kinetics in intracellular environments with macromolecular crowding: simulations and rate law. *Progress in Biophysics & Molecular Biology*, 85:235–260, 2004.
- [19] A. Minton. The influence of macromolecular crowding and macromolecular confinement on biochemical reactions in physiological media. *Journal of Biological Chemistry*, 276(14):10577–10580, 2001.
- [20] C. Cercignani. *The Boltzmann Equation and Its Applications*, Applied Mathematical Sciences, 67, Springer-Verlag, 1988.
- [21] I. Couzin, J. Krause, R. James, G. Ruxton, and N. Franks. Collective memory and spatial sorting in animal groups. *Journal of Theoretical Biology*, 218(1):1–11, 2002.
- [22] M. Born and H. Green. A general kinetic theory of liquids. I. The molecular distribution functions. *Proceedings of the Royal Society London A*, 188(1012):10–18, 1946.
- [23] J. Kirkwood. The statistical mechanical theory of transport processes I. General theory. *The Journal of Chemical Physics*, 14(3):180–201, 1946.
- [24] C. Cercignani, R. Illner, and M. Pulvirenti. *The Mathematical Theory of Dilute Gases*. Applied Mathematical Sciences, 106, Springer-Verlag, 1994.
- [25] T. Hillen. On the L^2 closure of transport equations: the Cattaneo approximation. *Discrete and Continuous Dynamical Systems B*, 4(4):961–982, 2004.
- [26] R. Erban and H. Othmer. From individual to collective behaviour in bacterial chemotaxis. *SIAM Journal on Applied Mathematics*, 65:361–391, 2004.
- [27] R. Erban and H. Othmer. From signal transduction to spatial pattern formation in *E. coli*: A paradigm for multi-scale modeling in biology. *Multiscale Modeling and Simulation*, 3:362–394, 2005.
- [28] B. Alder and T. Wainwright. Studies in molecular dynamics. I. General method. *The Journal of Chemical Physics*, 31(2):459–466, 1959.
- [29] G. Kremer. *An Introduction to the Boltzmann Equation and Transport Processes in Gases*. Springer-Verlag, 2010.
- [30] H. Sanchez-Arroyo. Largest Swarm. *Chapter 27, Book of Insect Records*. University of Florida 1997.
- [31] D. Sumpter. *Collective Animal Behavior*. Princeton University Press, 2010.
- [32] R. Erban. From molecular dynamics to Brownian dynamics. *Proceedings of the Royal Society A*, 470:20140036, 2014.
- [33] S. Chen and G. Doolen. Lattice Boltzmann method for fluid flows. *Annual Review of Fluid Mechanics*, 30:329–364, 1998.
- [34] For improved readability, we change the notation to $\mathbf{x} = \mathbf{x}^{(1)}$, $\mathbf{y} = \mathbf{x}^{(2)}$, $\mathbf{v} = \mathbf{v}^{(1)}$, $\mathbf{u} = \mathbf{v}^{(2)}$.

Appendix A: Approximation of (16)

Let us begin by analysing the part I_1 . Using the facts that $(\cdot)' : V \mapsto V$ is a bijection and $\mathbf{v}' \cdot \mathbf{n} = -\mathbf{v} \cdot \mathbf{n}$, we get

$$I_1 = - \int_V \int_V \int_{\mathbb{S}_+^1} (\mathbf{v}')' q(\mathbf{v}') q(\mathbf{u}') (\mathbf{v}' - \mathbf{u}') \cdot \mathbf{n} d\mathbf{n} d\mathbf{u} d\mathbf{v} = \int_V \int_V \int_{\mathbb{S}_+^1} \mathbf{v}' q(\mathbf{v}) q(\mathbf{u}) (\mathbf{v} - \mathbf{u}) \cdot \mathbf{n} d\mathbf{n} d\mathbf{u} d\mathbf{v}. \quad (\text{A1})$$

Integral I now takes the form

$$I = \int_V \int_V \int_{\mathbb{S}_+^1} (\mathbf{v}' - \mathbf{v}) q(\mathbf{v}) q(\mathbf{u}) (\mathbf{v} - \mathbf{u}) \cdot \mathbf{n} d\mathbf{n} d\mathbf{u} d\mathbf{v}.$$

For the reflective collisions defined in (2) we have $\mathbf{v}' - \mathbf{v} = -2(\mathbf{v} \cdot \mathbf{n})\mathbf{n}$ and we can simplify I to

$$I = -\frac{4}{3} \int_V \int_V \|\mathbf{v} - \mathbf{u}\| \mathbf{v} q(\mathbf{v}) q(\mathbf{u}) d\mathbf{u} d\mathbf{v}.$$

In order to evaluate this integral, we assume that $q(\mathbf{v})$ is close to an equilibrium, i.e. that we can write

$$q(\mathbf{v}) \approx \frac{\varrho}{|V|} + \delta g(\mathbf{v}), \text{ with } \delta \ll 1 \text{ and } g(\mathbf{v}) \sim \mathcal{O}(1). \quad (\text{A2})$$

This assumption is reasonable considering that the self-turning effect brings particle densities closer to equilibrium. We can plug this into the equation for I to obtain up to leading order:

$$I \approx -\frac{4\varrho}{3|V|} \delta \int_V \int_V \|\mathbf{v} - \mathbf{u}\| \mathbf{v} (g(\mathbf{v}) + g(\mathbf{u})) d\mathbf{u} d\mathbf{v},$$

where we use the fact that $\int_V \mathbf{v} d\mathbf{v} = \mathbf{0}$ and have dropped terms of order δ^2 . Using (4), we obtain the following two integral equalities for all $\mathbf{v} \in V$:

$$\int_V \|\mathbf{v} - \mathbf{u}\| d\mathbf{u} = 8s^2, \quad \int_V \|\mathbf{v} - \mathbf{u}\| \mathbf{u} d\mathbf{u} = -\frac{8s^2}{3} \mathbf{v}.$$

Consequently, using $|V| = 2\pi s$, we obtain

$$I \approx \frac{4\varrho}{3|V|} \left(8s^2 - \frac{8s^2}{3} \right) \delta \int_V \mathbf{v} g(\mathbf{v}) d\mathbf{v} = \frac{32s}{9\pi} \varrho \mathbf{m}^{(1)}, \quad (\text{A3})$$

where we have used

$$\mathbf{m}^{(1)} = \int_V \mathbf{v} p(\mathbf{v}) d\mathbf{v} = \delta \int_V \mathbf{v} g(\mathbf{v}) d\mathbf{v}.$$

Appendix B: Approximation of (21)

Repeating the steps we used to simplify integral (A1), we arrive at

$$J = \kappa\varepsilon \int_V \int_V \int_{\mathbb{S}_+^1} (\mathbf{v}' - \mathbf{v}) q(\mathbf{v}) (\mathbf{n} \cdot \nabla_{\mathbf{x}} q(\mathbf{u})) (\mathbf{v} - \mathbf{u}) \cdot \mathbf{n} d\mathbf{n} d\mathbf{u} d\mathbf{v}.$$

Using (2), we have $\mathbf{v}' - \mathbf{v} = -2(\mathbf{v} \cdot \mathbf{n})\mathbf{n}$. Integrating over $\mathbf{n} \in \mathbb{S}_+^1$, we obtain

$$J = -\kappa\varepsilon \frac{\pi}{4} \int_V \int_V \left(q(\mathbf{v}) (\mathbf{v} - \mathbf{u}) (\mathbf{v} \cdot \nabla_{\mathbf{x}} q(\mathbf{u})) + q(\mathbf{v}) \nabla_{\mathbf{x}} q(\mathbf{u}) (\mathbf{v} \cdot (\mathbf{v} - \mathbf{u})) + q(\mathbf{v}) \mathbf{v} ((\mathbf{v} - \mathbf{u}) \cdot \nabla_{\mathbf{x}} q(\mathbf{u})) \right) d\mathbf{u} d\mathbf{v}.$$

Employing approximation (A2) again, dropping terms of order $\mathcal{O}(\delta^2)$ and using $M^{(2)} \sim s^2 \varrho \mathbb{I}/2$, we obtain

$$J \approx -\kappa\varepsilon \frac{\pi}{2} M^{(2)} \nabla_{\mathbf{x}} \varrho - \kappa\varepsilon \frac{\pi s^2}{4} \varrho \nabla_{\mathbf{x}} \varrho \approx -\kappa\varepsilon \frac{\pi s^2}{2} \varrho \nabla_{\mathbf{x}} \varrho. \quad (\text{B1})$$